HHS Public Access

Author manuscript

JOM (1989). Author manuscript; available in PMC 2021 June 17.

Published in final edited form as:

JOM (1989). 2019 April 15; 71(4): 1281–1290. doi:10.1007/s11837-018-03325-3.

Self Assembled Recombinant Proteins on Metallic Nanoparticles As Bimodal Imaging Probes

ESRA YUCA, PH.D.[1,2], **CANDAN TAMERLER, PH.D.**[1,3,4,#]

[1]Institute for Bioengineering Research, University of Kansas, Lawrence-KS, 66045, USA

[2]Molecular Biology and Genetics, Yildiz Technical University, Istanbul 34210, Turkey

[3]Bioengineering Program, University of Kansas, Lawrence-KS, 66045, USA

[4]Mechanical Engineering, University of Kansas, Lawrence, KS 66045, USA

Abstract

Combining multiple modalities is at the center of developing new methods for sensing and imaging that are required for comprehensive understanding of events at the molecular level. Various imaging modalities have been developed using metallic nanoparticles owning to their exceptional physical and chemical properties. Due to their localized surface plasmon resonance characteristics, gold and silver nanoparticles exhibit unique optoelectronic properties commonly used in biomedical sciences and engineering. Self assembled monolayers or physical adsorption have previously been adapted to functionalize the surfaces of nanoparticles with biomolecules for targeted imaging. However, depending on differences among the functional groups used on the nanoparticle surface, wide variation in the displayed biomolecular property to recognize its target may result. In the last decade, the properties of inorganic binding peptides have been proven advantageous to assemble selective functional nano-entities or proteins onto nanoparticles surfaces. Herein we explored formation of self-assembled hybrid metallic nano-architectures that are composed of gold and silver nanoparticles with fluorescent proteins, for use as bimodal imaging probes. We employed metal binding peptide-based assembly to self assemble green fluorescence protein onto metallic substrates of various geometries. Assembly of the green fluorescent proteins, genetically engineered to incorporate gold- or silver-binding peptides onto metallic nanoparticles, resulted in the generation of hybrid-, biomodal-imaging probes in a single step. Green fluorescent activity on gold and silver surfaces can be been monitored using both plasmonic and fluorescent signatures. Our results demonstrate a novel bimodal imaging system that can be finely tuned with respect to nanoparticle size and protein concentration. Resulting hybrid probes may mitigate the limitation of depth penetration into biological tissues as well as providing high signal-to-noise ratio and sensitivity.

Keywords

Biomodal Imaging; Nanoparticles; Fluorescence proteins; Self-assembly; Metal Binding Peptides

[#] authors for correspondence ctamerler@ku.edu.

1. Introduction

There has been an adverse trade-off between sensitivity and selectivity for modality selection in imaging. Fluorescent imaging is a common method as it offers sensitivity, selectivity and versatility. While one form involves intrinsically fluorescent biochemical species, the other form covers the use of synthetic probes and nanomaterials to detect the molecular events that are not conforming for direct imaging [1, 2]. Inorganic nanoparticles (NP) with their instrinsic exceptional physical and chemical properties offer enhanced sensitivity with high resolution and as a result, they have been used as essential tools for imaging. Yet along, each imaging modality is limited by its own strength(s) and limitation(s) that impede a complete understanding of events at the molecular level. In contrast, bridging two or more imaging modalities can allow integration of their strengths while lowering their limitations. Hence combining multiple modalities has been at the center for developing advanced multimodal probes and methods needed for the next level of sensing and imaging [3–6].

Wavelength selective absorption and scattering abilities of gold and silver nanoparticles, as well as their surface plasmon resonance phenomena, have been used in applications ranging from biological imaging to molecular detection [7, 8]. At the nanoparticle-dielectric interface, localized oscillation of the induced plasmons provides a shorter decay length of the electromagnetic field and serve as an evanescent field around the nanoparticle. This produces a higher sensitivity to the differences in local refractive index changes between the absorbed layer on the surface and its local environment. Localized surface plasmon resonance (LSPR) commonly using gold and silver nanoparticles have been recognized as a label-free biosensing method that is sensitive and robust [9, 10]. While these inherent properties make LSPR a platform technology to be utilized in a wide range of applications, controlling the interfacial biomolecular interactions remains a challenge, as biofunctionalization onto the NP surfaces may result in wide variation to the display of the biomolecular functionality to recognize its target. [8].

Interface between inorganic materials and biomolecules brings additional challenges to control the orientation of biomolecules, as well as their spatial arrangement on the surface [11, 12]. When the biomolecule is near the surface of the material, the molecular orientation is critical to prevent variation in recognizing the target. Next-generation imaging and sensing technologies will immensely benefit from developing robust interfacial interactions having orientation control at the nanomaterial surface [13, 14].

The desired orientation of the various functional moieties, including fluorescent proteins, enzymes, antigens, and antibodies, onto specific surfaces is required to prevent variation in biomolecular function. Physical adsorption such as ionic, hydrophobic or polar interactions and chemical bonding processes using reactive side chains of biomolecules are among the numerous methods used for molecular immobilization on inorganic surfaces [15]. Proteins are commonly covalently attached to solid surfaces using the reactive groups that are located in the side chains of their component amino acids. Some of these groups may have an effect on the conformation of the proteins and cause the function of the protein to be reduced or even eliminated. Such chemical ligation reactions, among other complex chemical

processes, may lead to random protein immobilization and consequently limit its use for a desired application. Additionally, only a limited range of small molecules are used in surface functionalization, such as thiols for gold, silanes for silica or other oxides, and phosphonic acids for metal oxides. Self-assembled monolayers (SAMs) of thiol-based molecules have been frequently used for chemical and biological surface functionalization of metal surfaces [16–18]. On metal surfaces coated with SAMs via thiol chemistry, the biomolecules are chemically bonded to the SAM layer via reactive side chains, so that the SAMs become an intermediate molecular layer between the surface and the biomolecules [15]. Degradation due to oxidation on gold surfaces remains a significant limitation with these approaches.

Peptide-based molecular assemblers are becoming increasingly popular due to their ability to offer control over protein orientation with robust function owing to their 1) innate molecular recognition of materials, 2) self-assembly and 3) simplicity of combining with other biomolecules [19–24]. These peptides are commonly selected using combinatorial screening techniques, e.g. phage and cell surface display methods, for their specific binding interactions to inorganic substrate [25, 26]. Following their selection, further characterization experiments have been applied to determine their binding kinetics, thermodynamics and surface stability [24]. There have been several studies selecting new peptides as well as demonstrating their use, including assembly of nanoparticles (NPs) and biomolecules, designing bioactive surfaces or antimicrobial coatings, synthesis of inorganic materials, and developing nanostructured platforms [27–37]. Entrapment of the assembly of engineered proteins bound to the metal nanoparticles as well as minerals in the nanofibers was explored by integrating the fluorescent activity of the coupled proteins in the nanoassembly [38, 39]. Different processing methods have been investigated for controllable production [40] as well as printing with higher resolution onto metallic surfaces [41].

Herein, we investigated genetically engineered fluorescence fusion proteins that self assemble on metallic nanomaterials for use as bimodal imaging and sensing hybrid probes i.e. plasmonic and fluorescent with the added advantages that conditions for their use are environmentally and biologically benign. Gold binding (AuBP) and silver binding peptides (AgBP) demonstrating high binding affinity and specificity for gold and silver surfaces have been used as self-assembling peptide tags [42, 43]. Self-organization of green fluorescent protein (GFP) engineered incorporating AuBP and AgBP were investigated on various gold and silver surfaces. Binding kinetics and biological assays were performed to confirm the ability to control the protein orientation bound onto selected surfaces. Green fluorescent activity on gold and silver surfaces have been monitored using plasmonic and fluorescent activities as combined bimodality functions.

2. Materials and Methods

2.1. Construction of Recombinant Fusion Protein System: GFP-AuBP

The plasmid pGFP (Clontech, Takara Bio Inc., Mountain View, CA USA) was used as a template for polymerase chain reactions (PCR). Oligonucleotide primers were designed according to amino acid sequence of AuBP (CGP-WALRRSIRRQSY-GPC), linker (SGGG) and GFP fluorescent protein. A GFP-AuBP fusion protein encoding DNA fragment was obtained in four consecutive PCR reactions. Phusion High-fidelity DNA polymerase (NEB)

used for all PCR experiments. After double-digesting with *EcoRI-HindIII* restriction enzymes, GFP-AuBP encoding fragment ligated into the pMALc4x vector using a Quick Ligation Kit (NEB). Following DNA sequencing using ABI 3300 sequencer with BigDye terminator cycle sequencing kit (AB Applied Biosystems Inc., Carlsbad, CA, USA), the resulting plasmid construct was introduced into chemically competent *E. coli* ER2507 strains. Molecular structures for GFP and GFP-AuBP were visualized using UCSF Chimera software.

2.2. Expression and Purification of Engineered Recombinant Fusion Proteins

During the expression, we used maltose binding tag (MBP) as a single step purification tag for the recombinant protein system. Recombinant *E. coli* ER2507 bacteria harboring MBP-GFP,MBP-GFP-AuBP and MBP-GFP-AgBP encoding constructs were grown in LB medium (10 g/L Tryptone, 5 g/L Yeast Extract 5 g/L NaCl, pH 7) with 2 % glucose supplemented with 100 μg/mL ampicillin at 37 ºC with continuous shaking at 200 rpm. Bacterial expression was induced by adding 0.3 mM final concentration of IPTG (isopropyl-beta-D-thiogalactopyranoside) at OD_{600} of 0.6. After 16 hours incubation at 30 ºC the bacteria were harvested by centrifugation at 5,000g for 15 min at 4 ºC. Resuspended bacteria in column buffer (20 mM Tris-HCl, 200 mM NaCl, 1mM EDTA, pH 7.4) were sonicated five times (20 seconds each) at 200 W. The lysed cells centrifugated at 12,000 g for 30 minutes. Supernatant was filtered and loaded to pre-equilibrated amylose resin (NEB) column to purify the proteins having the maltose binding tag. Non-specific proteins were washed away with column buffer. Specifically bound recombinant fusion proteins were eluted by elution buffer (column buffer with 10 mM maltose). Purified protein samples were assessed by SDS-PAGE analysis.

Recombinant fuison proteins were next treated to remove the maltose binding purification tags. Centrifugal filter units with a molecular-weight cutoff of 10 kDa (Millipore) were used to concentrate the purified MBP-GFP and MBP-GFP-AuBP proteins. The buffer in the protein samples was replaced with another buffer containing 20 mM Tris-HCl, 100 mM NaCl, 2 mM $CaCl_2$ (pH 8.0) using the same filter units. 30 μg Factor Xa (NEB) was added to 1.5 mg fusion protein substrate. Following overnight incubation at 4 ºC each cleavage reaction sample was loaded onto the hydroxyapatite (Biorad) column which was prepared in 20 mM sodium phosphate, 200 mM NaCl (pH 7.2). Maltose molecules were washed away using the same buffer. MBP-bound protein samples, which was eluted with 0.5 M Na phosphate (pH 7.2), were loaded onto the amylose column. Protein samples without MBP affinity tag were obtained from the flow-through.

2.3. Physicochemical Properties and Spectrofluorophotometric Analyses

Isoelectric point (pI) and molecular weight (MW) of the proteins was calculated by ExPasy ProtParam tool. Fluorescence properties including optimal excitation and emission wavelengths and intensities were compared across purified protein samples using a spectrofluorophotometer (Shimadzu RF5301 PC).

2.5. Localized Surface Plasmon Resonance

Citrate-coated AuNPs (Ted Pella) were incubated with serial dilutions of GFP and GFP-AuBP proteins. Citrate-capped 15 nm AuNPs, which exhibit a characteristic LSPR maxima at 519 nm wavelength demonstrated a red-shift upon replacement of citrate by protein molecules. Binding and interaction properties of the fusion proteins to AuNP surfaces were compared with respect to their measured LSPR band shift.

2.6. Surface plasmon resonance (SPR) binding experiments

A four-channel SPR spectrometer (Radio Engineering Institute, Czech Republic) was used to characterize binding properties of the produced fusion proteins. All buffers were filtered through 0.2 μm pore size and degassed using ultrasonication for 20 minutes prior to use. Once a baseline was stabilized for each SPR channel, recombinant proteins in PBS were introduced to the gold sensor while the adsorption profile of the protein samples were monitored. All protein solutions (GFP, GFP-AuBP, MBP-GFP and MBP-GFP-AuBP) were introduced to the flow cell at a concentration of 0.1 μM.

2.7. Micro-contact Printing

Protein arrays consisted of MBP-GFP-AuBP were produced using micro-contact printing methods. MBP-GFP and MBP-GFP-AuBP proteins were applied to PDMS stamps for 10 min. After removing the excess proteins by washing, the PDMS stamps were gently dried with nitrogen. Protein-loaded PDMS stamps were then introduced to the gold surface. PDMS stamps were allowed to sit for 10 min. onto the gold surface and washed with DI water. Following a final step of gently drying the stamped surfaces with nitrogen, the protein arrays were imaged using a fluorescence microscope (Nikon, Japan) equipped with FITC filter.

2.8. Self-Assembly of GFP-AgBP2c on Silver Nanoparticle Arrayed Surface

Silver binding peptide-Glass binding fusion peptide (AgBP-GlBP) was microcontact printed on the glass cover slides. AgBP-GlBP printed substrate was incubated with 80 nm AgNP. After 30 minutes incubation, the substrates were washed and dried under nitrogen. The silver nanoparticle arrays were observed under dark field microscopy. Silver patterned surfaces were then incubated with MBP-GFP-AgBP2c and MBP-GFP proteins.

2.9. Fluorescence Tuning by Metal Nanoparticles

Fluorescent measurements were performed using TECAN Safire UV-Vis spectrometer microplate reader. Black-walled, flat-bottomed 384-well microplates (Corning) were used for sample preparation and measurement. Various concentrations of GFP-AuBP protein were incubated with 5 nm, 15 nm and 50 nm gold nanoparticles to achieve a total well volume of 50 μl. After incubation, fluorescence intensity was measured at 394 and 510 nm wavelengths for excitation and emission, respectively.

3. Results and Discussion

3.1. Production of Recombinant Fusion Proteins

Recombinant green fluorescent protein was developed as a fusion construct to incorporate gold binding peptide (GFP-AuBP). Primers were designed to include the amino acid sequence of AuBP with the linker sequence. GFP-AuBP encoding sequences were amplified using a series of forward and reverse primers containing extra residues including restriction enzyme site, i.e. *EcoRI* or *HindIII*, at their 5' ends, respectively. The DNA fragment encoding GFP-AuBP was obtained by consecutive polymerase chain reactions (PCR). The PCR product is expected to be approximately 790 base pairs. Molecular weight of the DNA fragments encoding the fusion and control proteins (no metal binding peptide tag) were confirmed using agarose gel electrophoresis (Figure 1). Since the expression vector, i.e. pMALc4x, encodes an maltose binding tag at the N-terminal, gold binding peptide (AuBP) sequence was incorporated at the C-terminal of the fusion fluorescent proteins to accommodate the bi-functionality. Cloning of GFP and GFP-AuBP fusion fragments into the expression vector was verified using both restriction and sequence analyses. Cloned genes were inserted into the expression vector downstream from the MBP encoding malE gene (Figure 1). Following the expression, each *E. coli* ER2507 culture expressing the multifunctional proteins were examined under UV light. Expression of the fusion protein incubation was found to be optimum when the culture was induced after 16 hours of growth at 30 ^{o}C.

3.2. Molecular and Structural Characterization of the Fusion Constructs

Engineered recombinant fusion green fluorescent proteins incorporated gold and silver binding peptides in addition to maltose binding protein tag (MBP). Maltose binding protein was chosen as a sugar binding protein fusion partner in our molecular construct. Periplasmic maltose binding proteins of bacteria have a role in uptake of sugars like maltose, maltotriose, and maltodextrins [44]. Maltose binding proteins have been cloned from *E. coli* and utilized in a variety of fluorescence-based biosensor systems [45–48]. Maltose binding protein also offers a unique advantage by lacking any cysteine residues and consequently it provides an ideal platform to prevents the sulfide-induced non-specific interaction of MBP with gold surface [20].

Figure 2a provides the engineered protein constructs with multi-functionality, MBP-GFP, MBP-GFP-AgBP and MBP-GFP-AuBP proteins. Expression vector included a specific sequence coding for the recognition site of a protease (Factor Xa). This recognition site allows to remove the maltose binding tag from the fusion proteins by carrying out a cleavage reaction following the purification step. After optimizing the expression conditions, we completed the protease cleavage. Next purity and molecular weights of the fusion proteins were assessed using a protein gel electrophoresis, i.e. SDS-PAGE (Figure 2b). A single, purified band was observed for each protein of interest confirming the production of the desired fusion green fluorescent proteins with gold or silver binding peptides.

Figure 3 provides the physicochemical properties of the purified proteins. Protein bands of MBP-GFP and MBP-GFP-AuBP were approximately at 70 kDa, GFP and GFP-AuBP were

at 30 kDa. Overall their molecular weight is comparable to their respective theoretical values. We next analyzed the excitation and emission properties of the purified proteins using fluorescence spectroscopy. MBP-tagged GFP-fusion proteins have similar excitation (394 nm) and emission (510 nm) wavelengths and intensities (Figure 3) as compared to that of GFP alone. Our results confirmed that fluorescence properties of GFP were protected upon the insertion of gold binding peptide and maltose binding protein tag.

3.3. Micro-patterning of Self Assembled Modular Fusion Proteins

Microcontact printing, a common soft-lithography technique, is an efficient approach for micropatterning of biomolecules [49, 50]. This approach has been used by different groups to pattern biological materials, such as proteins [51, 52], DNA molecules [53] and cells [54]. We used an original master template made of Polydimethylsiloxane (PDMS) mold. Once coated with proteins, the PDMS mold is pressed to make contact with a selected substrate surface to transfer the protein onto the surface. Gold binding peptide engineered into the multifunctional MBP-GFP-AuBP fusion protein enabled the self assembled formation of protein patterns on gold surfaces as shown in Figure 4. While microcontact printing guides the assembly of the protein samples on the surface, fluorescent labeling provides a visualization of the assembled proteins using a fluorescence microscope. Fluorescent labelling commonly requires additional labeling steps, whereas the method offered here allows to spot the location of the peptides or proteins in a single step by using the green fluorescence protein as a fusion partner in the protein assembly. Compared to control experiments (MBP-GFP), MBP-GFP-AuBP multifunctional protein resulted in a strong fluorescent intensity on the surfaces confirming gold binding peptide as essential component for the assembly process.

We next explored a hierarchical assembly through a layer by layer assembly of peptides, nanoaparticles and next recombinant fluorescent fusion. Schematic representation of the hierarchical assembly is provided in Figure 5. We designed and synthesized a bifunctional peptide that is composed of silver and glass binding peptide domains connected through a simple spacer region (AgBP-GlBP). Bifunctional AgBP-GlBP peptide enabled the self assembly of the silver nanoparticles onto glass surface. We also engineered silver binding peptides into the MBP-GFP fusion protein. Next MBP-GFP-AgBP fusion proteins were transferred on AgNPs decorated surfaces simply by pipetting and compared against MBP-GFP protein as a control. MBP-GFP-AgBP precisely assembled onto the nanoparticles arrays. The hierarchical self assembly achieved on the AgNPs using bifunctional peptides and recombinant fusion proteins confirms AgBP based guided assembly provides an orientation control over the formation hybrid arrays.

3.4. Fluorescent Protein Assembly Followed by Localized Surface Plasmon Resonance

Localized surface plasmon resonance (LSPR) has emerged as a label free technique to analyze biomolecular interactions. Local refractive index changes around the metallic nanoparticle can be measured by the sensitivity of the surface plasmon frequency. Althought the LSPR method is well established as a rapid and sensitive method, small biomolecules coating the nanoparticle surface as single film layer remains as an issue. We first cleaved the maltose binding protein from the multi-functional recombinant fusion fluorescent protein

constructs. Then we investigated the assembly and binding properties of GFP-AuBP onto metal, i.e. gold, nanoparticles using LSPR method. AuNPs were prepared at a final concentration of 40 μM and incubated with the fusion proteins for 2 hours. Next the absorbance spectra were recorded to calculate spectral peak shifts for each of the sample. Spectral shifts indicate an altered surface structure and size when AuNPs are successfully functionalized. The LSPR shifts observed at four different protein concentrations show that the GFP-AuBP hybrid protein binds to AuNP with a higher affinity than the control GFP. Higher protein concentration adsorption resulted in a higher red-shift supporting the consistent mass increase. This result suggests that a stable protein layer was formed on the surface of the nanoparticle following the incubation, with the increase in the nanoparticle size (Figure 6). Metal nanoparticles when they are functionalized with a biomolecule have been observed to result in UV-vis absorbance red-shifts and stimulated by the spacing and plasmonic coupling between nanoparticles [55–57].

3.5. Fluorescence Quenching on the Metal Nanoparticle Surface

Fluorescent quenching can be defined as the decrease in the intensity of the fluorescence. Due to principles of resonant energy transfer, when the fluorescent moiety interacts with a metal surface, the fluorescence intensity can be significantly quenched. We tested the potential quenching as a result of the interaction of the GFP-AuBP fusion protein with gold nanoparticles having sizes 5 nm, 15 nm and 50 nm. AuNPs were incubated with various concentrations of GFP-AuBP protein for 2 hours. Our results showed that as the protein concentration was increased, a greater fluorescence intensity (i.e., a lower quenching of GFP fluorescence) was observed. Surprisingly, when 2 μM of GFP-AuBP was applied to 15 nm AuNP, fluorescence level of the system was better controlled as compared to 50 nm AuNPs at the same protein concentration (Figure 7a). These results confirms that the fluorometric intensity is dependent upon NP size. To explore this as a platform technology, we next evaluated the fluorescence intensity of GFP-AgBP protein-functionalized AgNPs having sizes 20 and 80nm. Maintaining a constant AgNP concentration across both 20 and 80 nm sizes, we determined the fluorescence intensities of the GFP-AgBP/AgNP across various concentration of the fusion protein.

Fluorescence intensity or quenching capacity is highly dependent upon the distance between metal surface and the fluorophore. When this distance is constant, the quenching efficiency by the gold and silver nanoparticles then may depend upon properties such as the size and shape of the nanoparticle, the surface roughness, potential spectral overlap of the emission of the fluorophore molecule and nanoparticle absorption spectrum, or the molecular dipole orientation [58–62]. The effect of surface roughness on fluorescence intensity has been previously investigated to show that the fluorescence quenching ability may be enhanced due to the surface-damping effect below a critical intermolecular distance [62, 63]. Several studies aimed to reduce potential quenching by using an additional layer to separate the metal surface and the fluorophore molecule. Quenching also reported to be potentially controlled by tuning the spacer layer thickness [64–66]. Using a SiO_2 spacer in 5 nm thickness, Zhang, *et. al.*, (2012) obtained thousands-fold enhancements in fluorescence signal [67]. Proteins were also used as a biocompatible spacer layer [68]. Recently, fluorescence also has been shown to be regulated by employing a self-assembled monolayer

(SAM) of 1 nm or less thickness on the plasmo-photonic meta-surfaces [69]. However, degradation due to oxidation is a major limitation for the incorporation of SAMs on metal surfaces [70]. Our results shows that modularity of the GFP-AuBP and GFP-AgBP protein constructs allows being used as donor fluorescent molecules that could be applicable to a variety of applications including biosensing and bioimaging.

4. Conclusions

We demonstrated that green fluorescent protein (GFP) engineered to incorporate two different metal binding peptides, Au and Ag, can spontaneously form hierarchical hybrid assemblies on metal nanoparticles. Engineering fluorescent proteins to incorporate the metal binding peptide tags offered to formation of assemblies through biomolecular self assembly. As a result, plasmonic properties of gold and silver nanoparticles are combined with engineered fluorescent proteins as bimodal imaging probes in a single step. Our fluorescence bimodal imaging system combines both core metallic surface and finely tunable fluorescence features. Because of the robust β-barrel shape of GFP and specific binding and assembly of the solid binding peptides, our biocompatible system provides adjustable fluorescence and plasmonic features depending on the size of the nanoparticles and concentration of the protein constructs. The control of the interaction of metallic nanoparticles with biomolecules is critical for many biomedical applications, including imaging, diagnostic and therapeutic [71–76]. Multimodal imaging platforms composed of different imaging modalities can be further tailored towards specific targeting features using functionalized coatings [6].

Acknowledgements:

This study has been supported by The Scientific and Technological Research Council of Turkey (TUBITAK) BIDEB 2219 Post-Doctoral Research Project. This investigation was supported by Research Grant R01 DE025476 from the National Institute of Dental and Craniofacial Research, National Institutes of Health, Bethesda, MD 20892.

References

1. Misri R, Multimodality imaging, Molecular Imaging Techniques: New Frontiers, 2013, pp. 162–176.
2. Louie A, Chem. Rev, 110, 5(2010) doi:10.1021/cr9003538.
3. Fan QL, Cheng K, Hu X, Ma XW, Zhang RP, Yang M, Lu XM, Xing L, Huang W, Gambhir SS, Cheng Z, J. Am. Chem. Soc, 136, 43(2014) doi:10.1021/ja505412p.
4. Huynh E, Leung BYC, Helfield BL, Shakiba M, Gandier JA, Jin CS, Master ER, Wilson BC, Goertz DE, Zheng G, Nature Nanotechnology, 10, 4(2015) doi:10.1038/nnano.2015.25.
5. Li X, Kim J, Yoon J, Chen XY, Adv. Mater, 29, 23(2017) doi:10.1002/adma.201606857.
6. Zhao JH, Chen JW, Ma SN, Liu QQ, Huang LX, Chen XN, Lou KY, Wang W, Acta Pharmaceutica Sinica B, 8, 3(2018) doi:10.1016/j.apsb.2018.03.010.
7. Amendola V, Pilot R, Frasconi M, Marago OM, Iati MA, J Phys Condens Matter, 29, 20(2017) doi:10.1088/1361-648X/aa60f3.
8. Unser S, Bruzas I, He J, Sagle L, Sensors (Basel), 15, 7(2015) doi:10.3390/s150715684.
9. Austin LA, Mackey MA, Dreaden EC, El-Sayed MA, Arch. Toxicol, 88, 7(2014) doi:10.1007/s00204-014-1245-3.
10. Nicoletti O, de la Pena F, Leary RK, Holland DJ, Ducati C, Midgley PA, Nature, 502, 7469(2013) doi:10.1038/nature12469.

11. Wu LQ, Payne GF, Trends Biotechnol., 22, 11(2004) doi:10.1016/j.tibtech.2004.09.008.
12. Tamerler C, Surface Innovations, 4, 3(2016) doi:10.1680/jsuin.2016.4.3.109.
13. Kim DC, Kang DJ, Sensors, 8, 10(2008) doi:10.3390/s8106605. [PubMed: 27879693]
14. Cooper MA, Anal. Bioanal. Chem, 377, 5(2003) doi:10.1007/s00216-003-2111-y.
15. Rusmini F, Zhong Z, Feijen J, Biomacromolecules, 8, 6(2007) doi:10.1021/bm061197b.
16. Mrksich M, Whitesides GM, Annu. Rev. Biophys. Biomol. Struct, 25, (1996) doi:10.1146/annurev.bb.25.060196.000415.
17. Hoffmann PW, Stelzle M, Rabolt JF, Langmuir, 13, 7(1997) doi:10.1021/la961091+.
18. Bulusu A, Paniagua SA, MacLeod BA, Sigdel AK, Berry JJ, Olson DC, Marder SR, Graham S, Langmuir, 29, 12(2013) doi:10.1021/la303354t.
19. Sengupta A, Thai CK, Sastry MSR, Matthaei JF, Schwartz DT, Davis EJ, Baneyx F, Langmuir, 24, 5(2008) doi:10.1021/la702079e. [PubMed: 18047382]
20. Hnilova M, Karaca BT, Park J, Jia C, Wilson BR, Sarikaya M, Tamerler C, Biotechnol. Bioeng, 109, 5(2012) doi:10.1002/bit.24405.
21. Hnilova M, Khatayevich D, Carlson A, Oren EE, Gresswell C, Zheng S, Ohuchi F, Sarikaya M, Tamerler C, J. Colloid Interface Sci, 365, 1(2012) doi:10.1016/j.jcis.2011.09.006. [PubMed: 21978401]
22. Yuca E, Karatas AY, Seker UOS, Gungormus M, Dinler-Doganay G, Sarikaya M, Tamerler C, Biotechnol. Bioeng, 108, 5(2011) doi:10.1002/bit.23041.
23. Sarikaya M, Tamerler C, Schwartz DT, Baneyx FO, Annual Review of Materials Research, 34, (2004) doi:10.1146/annurev.matsci.34.040203.121025.
24. Tamerler C, Khatayevich D, Gungormus M, Kacar T, Oren EE, Hnilova M, Sarikaya M, Biopolymers, 94, 1(2010) doi:10.1002/bip.21368. [PubMed: 20091874]
25. Tamerler C, Oren EE, Duman M, Venkatasubramanian E, Sarikaya M, Langmuir, 22, 18(2006) doi:10.1021/la0606897. [PubMed: 16378392]
26. Tamerler C, Sarikaya M, Acta Biomater., 3, 3(2007) doi:10.1016/j.actbio.2006.10.009.
27. Walsh TR, Knecht MR, Chem. Rev, 117, 20(2017) doi:10.1021/acs.chemrev.7b00139.
28. Tanaka M, Hikiba S, Yamashita K, Muto M, Okochi M, Acta Biomater., 49, (2017) doi:10.1016/j.actbio.2016.11.037.
29. Munz M, Bella A, Ray S, Bell NC, Shard AG, Minelli C, Biointerphases, 11, 4(2016) doi:10.1116/1.4972417.
30. Adams B, Sarkes DA, Finch AS, Stratis-Cullum D, Advances in synthetic peptides reagent discovery, 2013.
31. Gazit E, Annu. Rev. Biochem, 87, 1(2018) doi:10.1146/annurev-biochem-062917-012541. [PubMed: 29925256]
32. Tamerler C, Dincer S, Heidel D, Hadi Zareie M, Sarikaya M, Prog. Org. Coat, 47, 3(2003) doi:10.1016/j.porgcoat.2003.08.014.
33. Hnilova M, So CR, Oren EE, Wilson BR, Kacar T, Tamerler C, Sarikaya M, Soft Matter, 8, 16(2012) doi:10.1039/C2SM06426J.
34. Demir HV, Seker UOS, Zengin G, Mutlugun E, Sari E, Tamerler C, Sarikaya M, ACS Nano, 5, 4(2011) doi:10.1021/nn103127v.
35. Zhou Y, Snead ML, Tamerler C, Nanomedicine, 11, 2(2015) doi:10.1016/j.nano.2014.10.003.
36. Yazici H, Habib G, Boone K, Urgen M, Utku FS, Tamerler C, Materials Science and Engineering: C, 94, (2019) doi:10.1016/j.msec.2018.09.030.
37. Yucesoy DT, Hnilova M, Boone K, Arnold PM, Snead ML, Tamerler C, JOM (Warrendale, Pa. : 1989), 67, 4(2015) doi:10.1007/s11837-015-1350-7.
38. Wu X, Mahalingam S, VanOosten SK, Wisdom C, Tamerler C, Edirisinghe M, Macromol. Biosci, 17, 2(2017) doi:10.1002/mabi.201600270.
39. Zhang SQ, Karaca BT, VanOosten SK, Yuca E, Mahalingam S, Edirisinghe M, Tamerler C, Macromol. Rapid Commun, 36, 14(2015) doi:10.1002/marc.201500174.
40. Heseltine PL, Ahmed J, Edirisinghe M, Macromolecular Materials and Engineering, 303, 9(2018) doi:10.1002/mame.201800218.

41. Hashimdeen SH, Miodownik M, Edirisinghe MJ, Materials Science & Engineering C-Materials for Biological Applications, 33, 6(2013) doi:10.1016/j.msec.2013.04.020.
42. Hnilova M, Oren EE, Seker UOS, Wilson BR, Collino S, Evans JS, Tamerler C, Sarikaya M, Langmuir, 24, 21(2008) doi:10.1021/la801468c.
43. Hnilova M, Liu X, Yuca E, Jia C, Wilson B, Karatas AY, Gresswell C, Ohuchi F, Kitamura K, Tamerler C, Acs Applied Materials & Interfaces, 4, 4(2012) doi:10.1021/am300177t.
44. Shilton BH, Flocco MM, Nilsson M, Mowbray SL, J. Mol. Biol, 264, 2(1996) doi:10.1006/jmbi.1996.0645.
45. Allen MW, Urbauer RJ, Zaidi A, Williams TD, Urbauer JL, Johnson CK, Anal. Biochem, 325, 2(2004).
46. Le NCH, Gel M, Zhu YG, Dacres H, Anderson A, Trowell SC, Biosens. Bioelectron, 62, (2014) doi:10.1016/j.bios.2014.06.032.
47. Fehr M, Frommer WB, Lalonde S, Proc. Natl. Acad. Sci. U. S. A, 99, 15(2002) doi:10.1073/pnas.142089199.
48. Ha JS, Song JJ, Lee YM, Kim SJ, Sohn JH, Shin CS, Lee SG, Appl. Environ. Microbiol, 73, 22(2007) doi:10.1128/aem.01080-07. [PubMed: 17056689]
49. Dias A, Kingsley D, Corr D, Biosensors, 4, 2(2014).
50. Ruiz SA, Chen CS, Soft Matter, 3, 2(2007) doi:10.1039/b613349e.
51. Bernard A, Delamarche E, Schmid H, Michel B, Bosshard HR, Biebuyck H, Langmuir, 14, 9(1998) doi:10.1021/la980037l.
52. Kacar T, Ray J, Gungormus M, Oren EE, Tamerler C, Sarikaya M, Adv. Mater, 21, 3(2009) doi:10.1002/adma.200801877.
53. Lange SA, Benes V, Kern DP, Horber JKH, Bernard A, Anal. Chem, 76, 6(2004) doi:10.1021/ac035127w.
54. Mrksich M, Dike LE, Tien J, Ingber DE, Whitesides GM, Exp. Cell Res, 235, 2(1997) doi:10.1006/excr.1997.3668.
55. Unser S, Holcomb S, Cary R, Sagle L, Sensors, 17, 2(2017) doi:10.3390/s17020378.
56. Joshi D, Soni RK, Plasmonics, 13, 4(2018) doi:10.1007/s11468-017-0633-y.
57. Ben Haddada M, Hu D, Salmain M, Zhang L, Peng C, Wang Y, Liedberg B, Boujday S, Anal. Bioanal. Chem, 409, 26(2017) doi:10.1007/s00216-017-0563-8.
58. Lakowicz JR, Anal. Biochem, 337, 2(2005) doi:10.1016/j.ab.2004.11.026.
59. Pineda AC, Ronis D, J. Chem. Phys, 83, 10(1985) doi:10.1063/1.449695.
60. Dulkeith E, Morteani AC, Niedereichholz T, Klar TA, Feldmann J, Levi SA, van Veggel FCJM, Reinhoudt DN, Möller M, Gittins DI, Phys. Rev. Lett, 89, 20(2002).
61. Dulkeith E, Ringler M, Klar TA, Feldmann J, Muñoz Javier A, Parak WJ, Nano Lett., 5, 4(2005) doi:10.1021/nl0480969.
62. Swierczewska M, Lee S, Chen X, Phys. Chem. Chem. Phys, 13, 21(2011) doi:10.1039/C0CP02967J.
63. Leitner A, Lippitsch ME, Draxler S, Riegler M, Aussenegg FR, Appl. Phys. B, 36, 2(1985) doi:10.1007/bf00694696.
64. Schneider G, Decher G, Nerambourg N, Praho R, Werts MHV, Blanchard-Desce M, Nano Lett., 6, 3(2006) doi:10.1021/nl052441s.
65. Cheng D, Xu Q-H, Chem. Commun, 3(2007) doi:10.1039/B612401A.
66. Wang X, He F, Zhu X, Tang F, Li L, Sci. Rep, 4, (2014) doi:10.1038/srep04406
67. Weihua Z, Fei D, Wen-Di L, Yuxuan W, Jonathan H, Stephen YC, Nanotechnology, 23, 22(2012).
68. Tang F, Wang C, Wang X, Li L, Colloids Surf. Physicochem. Eng. Aspects, 485, (2015) doi:10.1016/j.colsurfa.2015.09.010.
69. Choi B, Iwanaga M, Miyazaki HT, Sugimoto Y, Ohtake A, Sakoda K, Chem. Commun, 51, 57(2015) doi:10.1039/c5cc04426j.
70. Mani G, Johnson DM, Marton D, Dougherty VL, Feldman MD, Patel D, Ayon AA, Agrawal CM, Langmuir, 24, 13(2008) doi:10.1021/la8003646.

71. Duran N, Duran M, de Jesus MB, Seabra AB, Favaro WJ, Nakazato G, NanomedicineNanotechnology Biology and Medicine, 12, 3(2016) doi:10.1016/j.nano.2015.11.016.

72. Zhang XF, Liu ZG, Shen W, Gurunathan S, Int. J. Mol. Sci, 17, 9(2016) doi:10.3390/ijms17091534.

73. Lara HH, Garza-Trevino EN, Ixtepan-Turrent L, Singh DK, Journal of Nanobiotechnology, 9, (2011) doi:10.1186/1477-3155-9-30.

74. Tan XX, Wang JP, Pang XJ, Liu L, Sun Q, You Q, Tan FP, Li N, Acs Applied Materials & Interfaces, 8, 51(2016) doi:10.1021/acsami.6b11262.

75. Zhang XY, Cell Biochem. Biophys, 72, 3(2015) doi:10.1007/s12013-015-0529-4.

76. Zhang Q, Gong Y, Guo XJ, Zhang P, Ding CF, Acs Applied Materials & Interfaces, 10, 41(2018) doi:10.1021/acsami.8b12897.

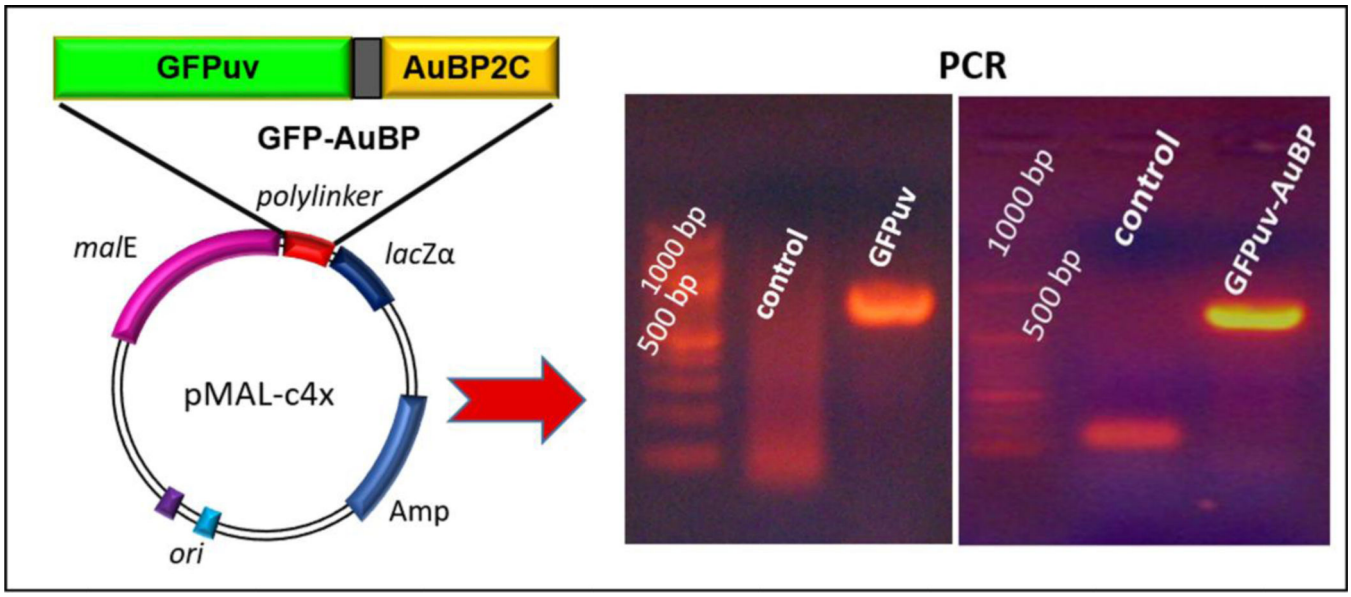

Figure 1.

Schematic representation of MBP-GFP-AuBP encoding genetic construct and DNA fragments amplified with Phusion High-fidelity DNA polymerase (NEB). Lane 1: O'RangeRuler 50 bp DNA Ladder (Thermo Scientific), lane 2: Negative control, lane 3: GFP-AuBP and GFP encoding DNA fragment.

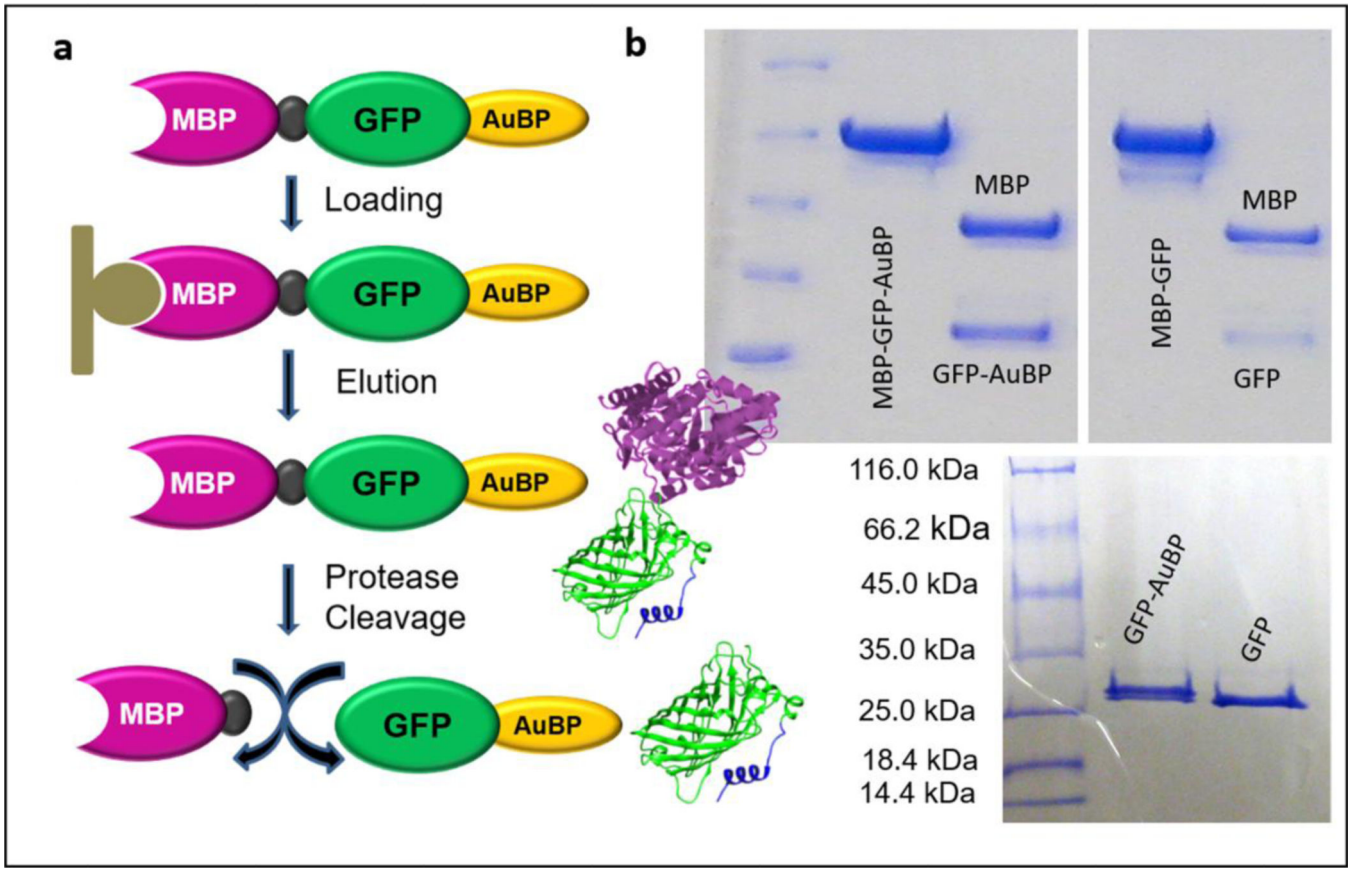

Figure 2.

(a). Schematic illustration for GFP-AuBP purification (b) SDS-PAGE analysis of purified, cleaved and uncleaved MBPGFP-AuBP and MBP-GFP proteins. Following purification of MBP-GFP-AuBP and MBP-GFP fusion proteins, MBP tags were cleaved by Factor Xa and then removed by subsequent chromatography steps.

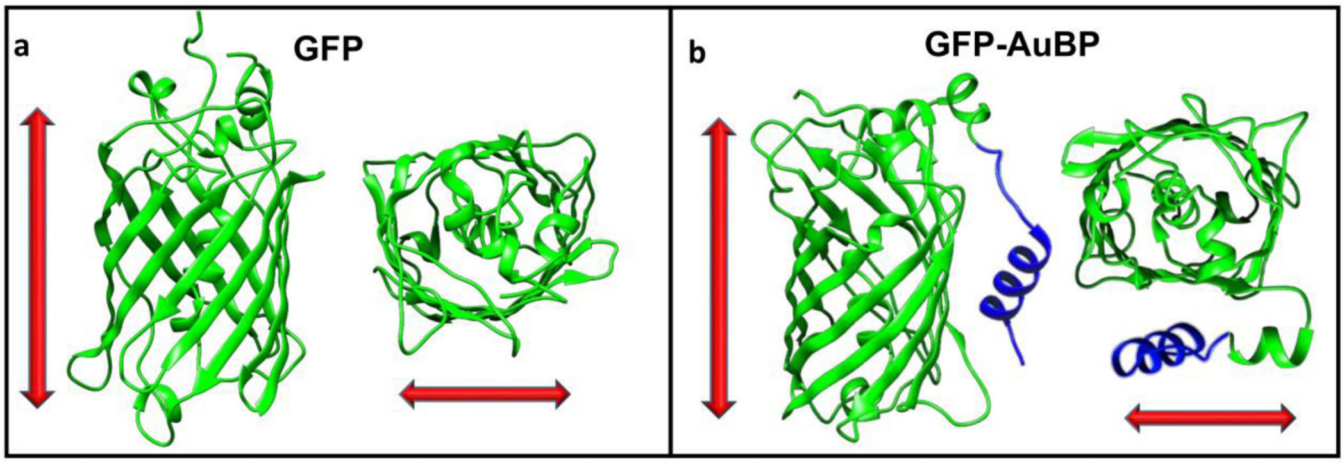

c

Protein	Number of Amino Acids	pI	MW (kDa)
MBP-GFP	629	5.33	69.764
GFP	242	5.68	27.272
MBP-GFP-AuBP	651	5.55	72.111
GFP-AuBP	264	6.22	29.619

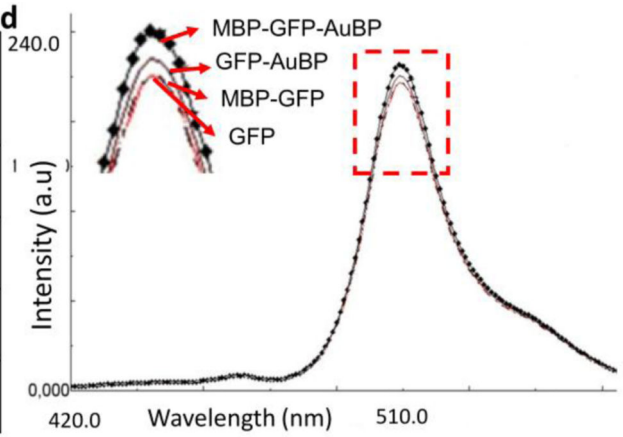

Figure 3.
(a) Molecular structure of GFP and (b) GFP-AuBP, (c) Physicochemical properties of the recombinant proteins, (d) Emission spectra for the purified proteins.

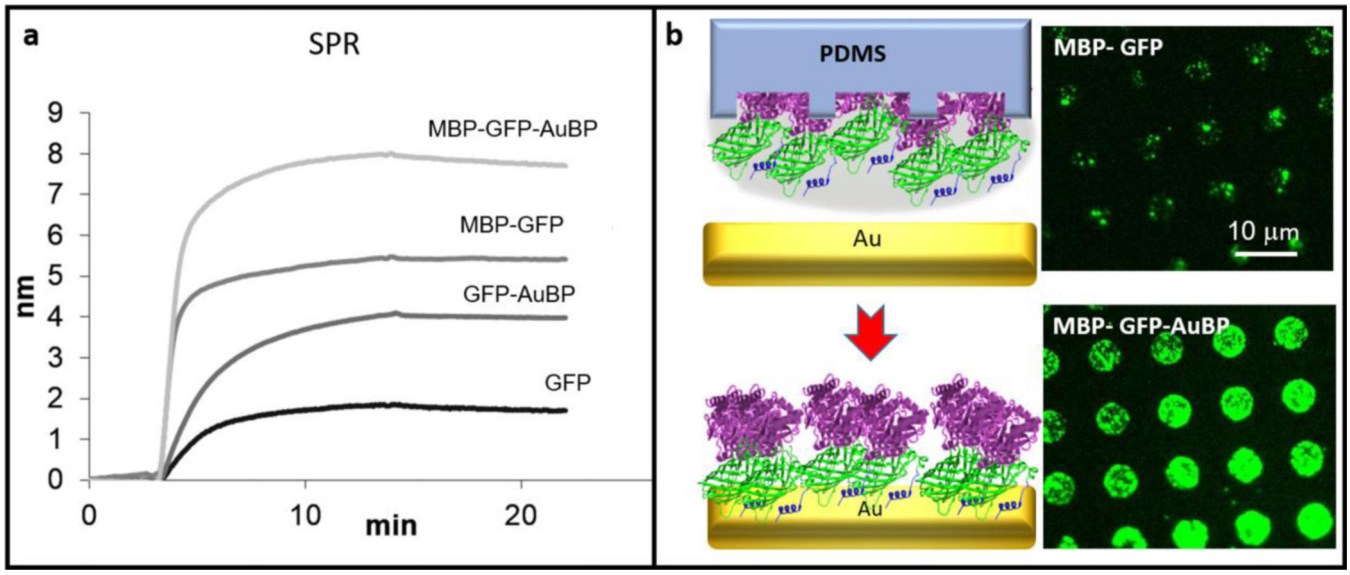

Figure 4.

(a) SPR determines the specificity of the binding. SPR sensorgrams recorded for purified MBP-GFP, MBP-GFP-AuBP, GFP and GFP-AuBP. (b) Schematic of protein patterning and FM images of micro-contact printing of 8 µM MBP-GFP-AuBP protein on flat gold surface via PDMS stamping. MBP-GFP, lacking the AuBP peptide, was used as a control.

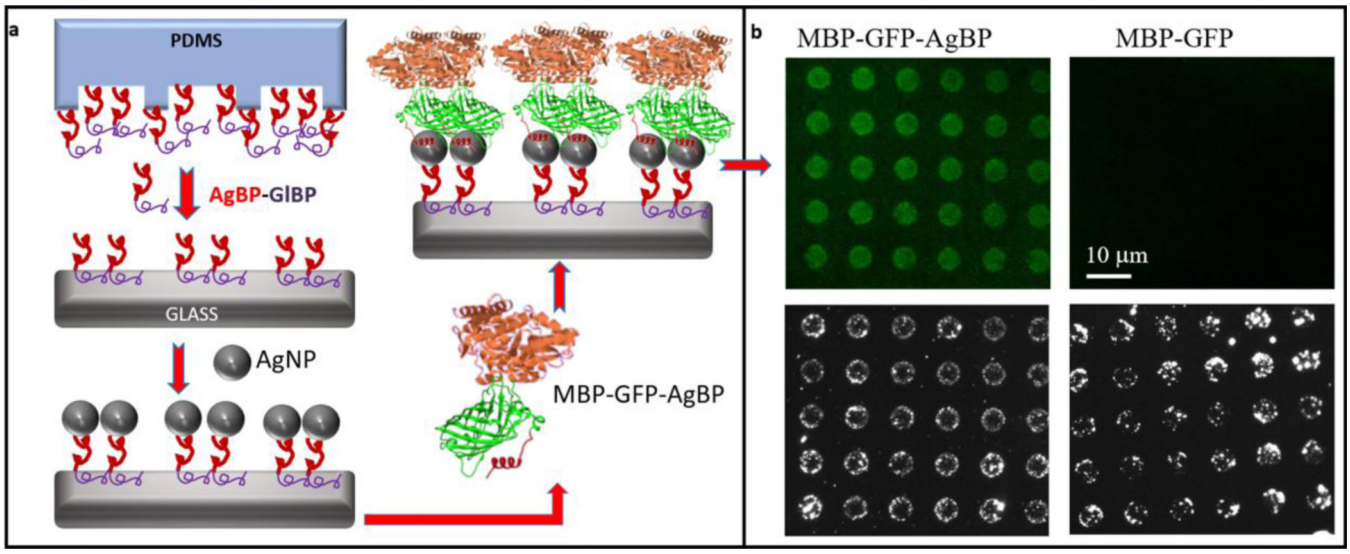

Figure 5.

(a) Schematic of micropatterning formed through PDMS stamping of bifunctional peptide composed of silver and glass binding peptide domains (AgBP-GlBP) followed by silver nanoparticle assembly and the micropatterns incubated with multi-functional fusion protein (MBP-GFP-AgBP). (b) Fluorescence (upper) and dark field images of the micropattern formed through PDMS stamping of AgBP-GBP followed by silver nanoparticle assembly and the micropatterns incubated with 15 μM MBP-GFP-AgBP (left) and MBP-GFP proteins.

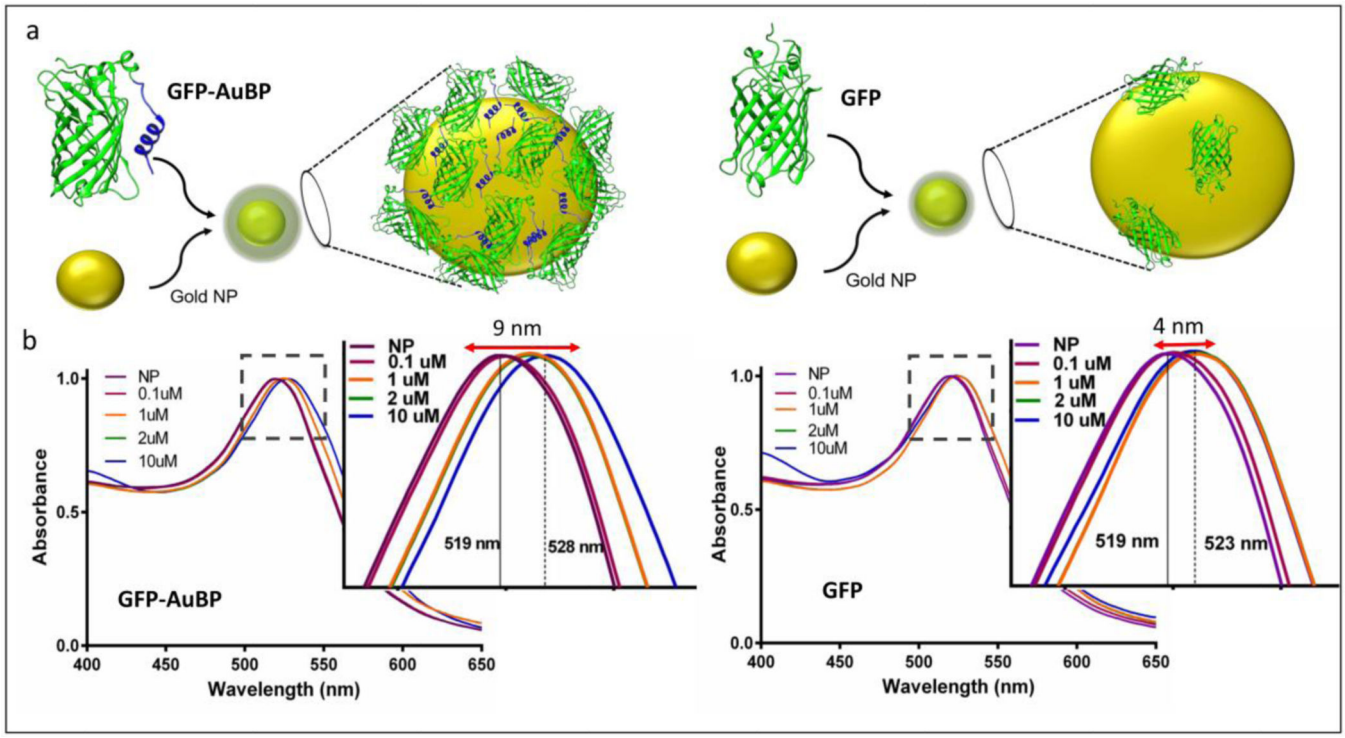

Figure 6.

(a) Schematic illustration of the AuNP functionalization with gold binding fusion protein GFP-AuBP. (b) Localized surface plasmon resonance (LSPR) spectra of fluorescent protein functionalized AuNPs. Spectral peaks collected after 16 h of incubation with GFP-AuBP and GFP protein. A red shift was observed due to increased protein concentration.

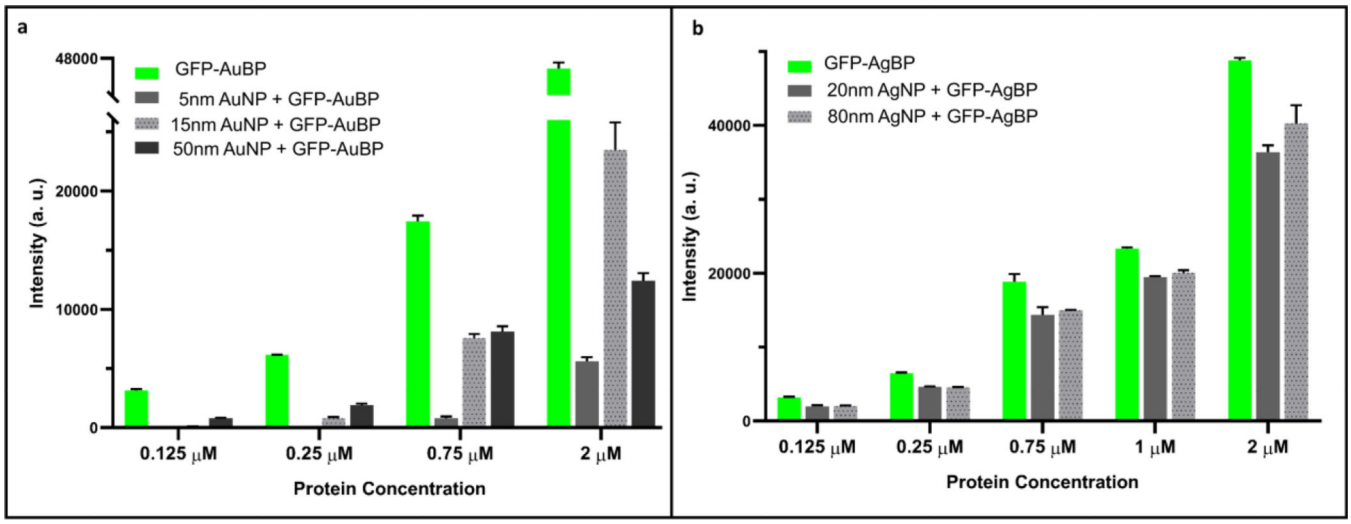

Figure 7.

Fluorescence Intensity on (a) GFP-AuBP proteins bound to 5 nm, 15 nm and 50 nm AuNPs. (b) GFP-AgBP proteins bound to 20 nm and 80 nm AgNPs.